4

Three-Dimensional Silicon Smart Tactile Imager Using Large Deformation of Swollen Diaphragm with Integrated Piezoresistor Pixel Circuits

Hidekuni Takao and Makoto Ishida
Toyohashi University of Technology
Japan

1. Introduction

Recently, various kinds of tactile sensors have been investigated and reported for tactile applications with robot fingertips. Typical specifications of human fingertips are known as follows; spatial resolution of human fingertip is around 1 mm, time resolution is below 1 msec (1 kHz), and the minimum force resolution is around 1-10 mN. Also, human fingertip can recognize the three-dimensional (3-D) shape of touching object using flexible deformation in the convex shape of fingertip skin. However, it is very difficult to realize all the above requirements/performances in conventional tactile sensors at the same time.

Tactile imager is a spatial distribution type of sensor, which can detect the object contact force and its distribution with an array of force or pressure sensors. In addition, detection ability of 3-D surface shape will be required for object handling. Tactile imagers can be applied to robot applications such as in robots for the assistance of visually handicapped and so on. There are two major trends in the previously reported tactile imagers. One is the polymer-based tactile imager realized by the substrate with organic materials, and the other one is silicon-MEMS type sensors. In polymer-based tactile imagers (Brussel & Belien, 1986; Engel et al., 2003; Shimojo et al., 2004; Someya et al., 2004, Engel et al., 2005), pressure-sensitive conducting rubber has generally been used as a major force sensing element (Brussel & Belien, 1986; Shimojo et al., 2004; Engel et al., 2005). Polymer-based sensors are suitable for wide area tactile sensors since the fabrication cost per unit area is considered to be much lower than that of silicon sensors. Artificial skin mounted on large areas of robot surface is one of the major applications (Someya et al., 2004; Engel et al., 2005). Essential disadvantages of polymer-based sensors are relatively low spatial resolution and upper limitation on the number of pixels due to electronic signal wires. Typical spatial resolution of polymer-based tactile imagers is around 2 ~ 4 mm range, which is not high enough for fingertip tactile sensing applications as mentioned below. Although a tactile imager with a large number of pixels has been reported using organic-FET switching matrix (Someya et al., 2004), it still utilizes conducting rubber sensor elements. Also, the integration density of organic-FET is much lower than the present silicon technology, and its long term reliability in force sensor applications has not yet been demonstrated.

Silicon-MEMS tactile imagers, integrating micro pressure sensor array (Sugiyama et al., 1990) or micro force-sensor array, have been reported earlier (Suzuki et al., 1990(a); (b);

Source: Sensors, Focus on Tactile, Force and Stress Sensors, Book edited by: Jose Gerardo Rocha and Senentxu Lanceros-Mendez, ISBN 978-953-7619-31-2, pp. 444, December 2008, I-Tech, Vienna, Austria

Kobayashi et al., 1990; Souza & Wise, 1997; Mei et al., 1999; Mei et al., 2000; Sato et al, 2003; Charlot et al, 2004). This type of sensors can reduce the number of electronic signal wires by integrated switching matrix fabricated using CMOS technology (Doelle et al, 2004). Also, processing circuits can be integrated for front-end signal processing of the pixel array. As compared to the polymer-based tactile imagers, a higher spatial resolution can be realized using silicon micromachining. 500 dpi spatial resolution has already been reported (Souza & Wise, 1997), and such sensors with high spatial resolutions can be used for fingerprint identification (Sato et al., 2003; Charlot et al., 2004). Most of the silicon tactile imagers are configured as integrated array of individual micromechanical sensor structures. Piezoresistive or capacitive sensors are fabricated in each pixel structure. Since movable stroke of such micro pixels is usually very short (~1μm), it is difficult to realize flexible sensor surface to detect 3-D surface shape of touching object. In order to solve the problem, thick and protective layer of elastomer can be coated on the sensor array. However, such soft materials usually have nonlinearity due to creep and hysteresis in mechanical response. In addition, thick and soft layer works as spatial low-pass filter for the high density pixel array, which degrades the spatial resolution of original sensors. Although silicon-MEMS tactile sensors can realize higher spatial resolution, it is difficult to realize surface flexibility.

Fig. 1. A future image of tactile imager embedded in robot fingers. They will function as artificial tactile sense of fingertips in human-coexistence type robots.

Considering the tactile sensing in human-coexistence type robots, tactile imagers like human fingertip will be required in near future. Figure 1 shows an image of tactile imager embedded in robot fingers. The embedded imagers will function as artificial tactile sense of fingertips in human-coexistence type robots. In human fingertips, a large number of highly sensitive tactile corpuscles are distributed under skin, and their surface has flexibility for object contact. As explained, it is difficult for previously reported tactile imagers to satisfy the requirements for fingertip applications. In this study, a novel concept of silicon-MEMS tactile imager aimed at fingertip tactile application and the evaluation results of a fabricated device are presented. The final target is multi-functional integrated tactile imager with force, temperature, and vibration sensing elements in sensor arrays as shown in Fig. 1, since silicon technology is very suitable to integrate many kinds of functional sensors/circuits. In this concept, pneumatically swollen single silicon diaphragm integrated with a two-dimensional (2-D) array of strain-sensitive resistors (piezoresistors) is used for tactile sensor

array instead of individually separated micromechanical sensor array. This structure has both the large number of pixels and surface flexibility for 3-D object contact (Takao et al., 2004; 2006). The surface shape similar to the diaphragm mechanical stroke can be detected as 3-D information (2-D position in array and depth information). In addition, spatial resolution higher than the polymer-based tactile imagers can be realized. A single tactile sensor with air pressure control has been proposed earlier to detect object hardness (Hasegawa et al., 2003). Air pressure is used to realize elastic surface and mechanical controllability of the surface of sensing area. In this chapter, the new concept, principle, design and experiments are presented in detail.

2. Configuration of tactile imager with silicon-LSI

2.1 A new concept of flexible silicon tactile Imager

In order to realize large mechanical stroke of tactile imager, this device concept uses large deformation of silicon diaphragm. Figures 2 (a) and (b) show schematic diagrams of the silicon tactile-force imager proposed in this study. It consists of three major components; (1) silicon diaphragm with sensing pixel array for contact force imaging, (2) signal processing circuitry integrated with IC technology, and (3) pressure chamber under the sensing diaphragm. 2-D piezoresistor pixel array is integrated on the thin silicon diaphragm. Each

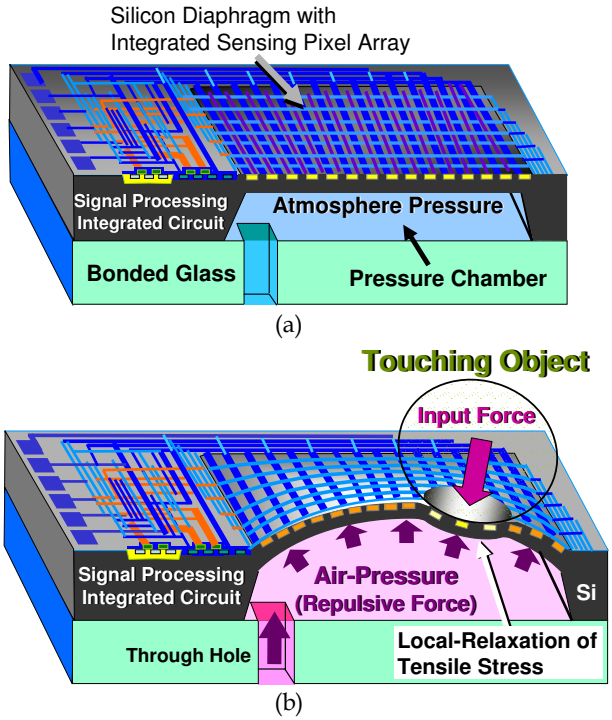

Fig. 2. Schematic diagrams of the tactile imager with skin-like sensing area; (a) Diaphragm backside pressure is equal to atmosphere pressure, (b) Diaphragm is swollen by a pressure, and set in the detection mode of tactile sensing.

strain-sensor pixel is electrically isolated, but, is not isolated mechanically, since all the pixels are formed on a continuous thin diaphragm structure. Switching and signal processing circuits for the sensing pixel array are monolithically integrated around the sensing diaphragm region. Pressurized air is provided to the chamber through the hole in the glass in order to apply the pressure to the diaphragm backside. In Fig. 2 (a), pressure on the diaphragm backside is equal to the atmosphere pressure, and the diaphragm is kept flat. If pressurized air is applied to the diaphragm backside, the diaphragm is deformed and swollen upward like a balloon as shown in Fig. 2 (b). Displacement of the swollen diaphragm depends on the dimensions and applied pressure, and a movable stroke of around 10~200 μm can easily be realized in this approach. Advantages of the tactile imager with pneumatically swollen single diaphragm structure are summarized below.

a. Flexibility of the sensor surface is obtained without any elastomeric materials for high spatial resolution. Convex shape of the swollen surface makes it easier to contact with the sensing target like human's fingertips.
b. Swollen large diaphragm can realize large stroke of surface indentation. 3-D surface shape can be detected by measuring the indentation depth (force) of the swollen diaphragm surface.
c. Pixel pitch of the strain sensor array can be made smaller compared to the polymer-based sensors. In addition, number of pixels in the sensor array can be larger with processing ability of the integrated circuits.
d. Stiffness of the sensing region of diaphragm can be controlled by the backside pressure. This means that characteristics of the sensor can be controlled even after the device packaging is completed (Fig. 2(b)).

2.2 Principle of 3-D Tactile Imaging

In this sensor, contact force image corresponding to 3-D image of the surface shape is detected by reading the stress distribution change on the swollen diaphragm using the 2-D piezoresistor pixel array. Figure 3 shows a cross-sectional view of the detection principle of this tactile imager. The number of piezoresistor pixel array and the pixel pitch can be changed in alternative designs. It mainly depends on the feature size of CMOS fabrication technology used. In the initial state, before the object contact, shown in Fig. 3 (a), tensile membrane stress is distributed with uniform amplitude over the entire piezoresistor array on the diaphragm. Since the swollen silicon diaphragm has a finite thickness, bending stress is generated in addition to the tensile membrane stress on the diaphragm. The surface stress on diaphragm appears according to the principle of superposition of the two components. Tensile membrane stress is caused by the large deformation of diaphragm, and bending stress is caused by the bending moment proportional to the distance from the neutral plane in the diaphragm. If the backside pressure is high, bending stress is negligible as compared to tensile membrane stress (i.e. initial stress on the array can be regarded as uniform value). However, the ratio between the membrane stress and the bending stress becomes only 5 or less depending on the backside pressures in the case of 10 μm diaphragm thickness. In order to cancel out the offset distribution caused by the effect of bending moment, they are once memorized, and subtracted from the output for zero point adjustment. This operation can be performed by software in the measurement system.

Figure 3 (b) shows the sensing mode of contact force of the object. If a hard object touches the surface of the sensing region, swollen diaphragm is deformed at the object contacting

points as shown in Fig. 3 (b). Diaphragm region where the object is in contact is pushed downward, and the tensile membrane stress applied initially around the contacting object is eased and reduced by the local deformation causing compressive bending stress around the contacting points. Difference of stress distribution from the initial state corresponds to the signal of the tactile imager, and it can be read out from the 2-D piezoresistor pixel array sequentially. Also, the image corresponds to the depth distribution of the touching object. Thus, the signal component shows peaks at around the tips of contacting object, and the positions and amplitudes of force (i.e. indentation depth) on the diaphragm can be detected as 3-D shape image of the touching object based on this principle.

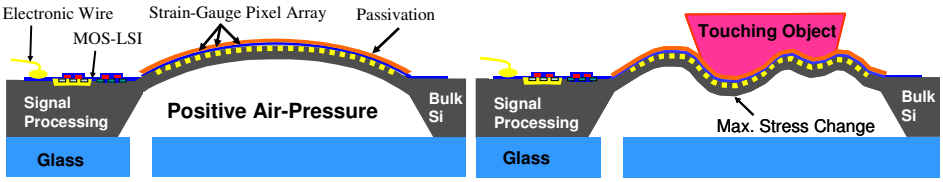

(a) (b)

Fig. 3. Detection principle of the tactile imager with surface stress distribution on the diaphragm; (a) Initial state before object touching, (b) 3-D shape detection with deformation.

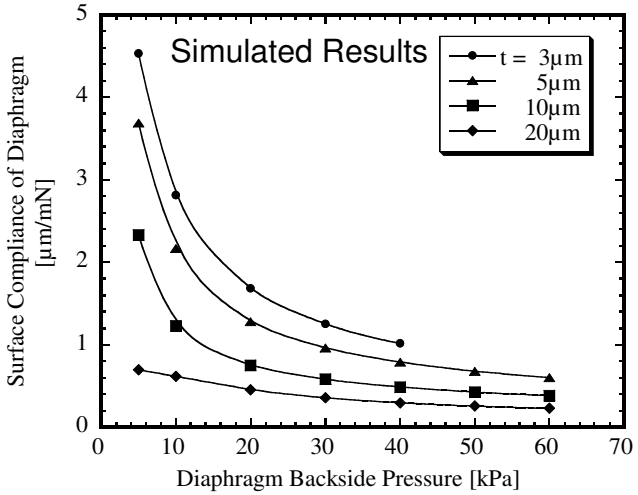

Fig. 4. Simulated surface compliance of pneumatically swollen single-crystal silicon diaphragm for various thicknesses. FEM non-linear analysis was performed for simulations.

Mechanical properties of the sensing diaphragm can be controlled by changing the backside air pressure. For example, compliance of the swollen diaphragm strongly depends on the backside pressure. Finite Element Method (FEM) non-linear analysis was performed to analyze the mechanical property of swollen diaphragm using ANSYS®. Total area of the simulated diaphragm is 3040×3040 μm², and the edges are fixed to the silicon substrate like a structure shown in Fig. 2 (a). Figure 4 shows a simulated relationship between the surface compliance of diaphragm and backside air pressure for various diaphragm thicknesses.

Force is applied at a point on the diaphragm surface in the FEM simulation. If the thickness of diaphragm increases, dependence of the surface compliance on the backside pressure becomes small due to its own rigidity as seen in the figure. It is considered from the result that thinner diaphragm is advantageous for controlling the characteristics of tactile imager. Assuming that the thickness of diaphragm is same, higher sensitivity can be obtained with lower backside pressure since the surface stiffness becomes lower and surface stress change will be increased for the same contact force. Conversion factor from the input force into stress change on a pixel is a dominant factor in the force sensitivity of tactile imager. On the other hand, upper limit of the detectable force can be increased by the increased backside pressure. Simulated dependence of the sensitivity and input force range on the pressure are compared with the measured results in a later section.

Spatial resolution of the contact force distribution cannot be determined only by the pitch of piezoresistors. Since the pixels are not mechanically isolated from each other, there is some crosstalk of strain among piezoresistor pixels. If the pixel pitch of piezoresistors is shorter than the effective limit of mechanical crosstalk, spatial resolution of the tactile imager is limited by the crosstalk effect. FEM non-linear analysis was performed to estimate the crosstalk between the multiple force input positions. Figure 5 (a) shows the parameters used in the simulation. Diaphragm size used in the FEM simulation is the same as in the case of Fig. 4 (3040×3040 μm2). Simulation was performed for different distances 'd', of two input forces, varying from 120 μm to 1200 μm. In order to evaluate the spatial resolution, stress change from the initial state (signal component) generated by the two forces is plotted as a function of distance from the center of two forces as shown in Fig. 5 (b). In the simulation result, amplitude of the applied forces is 5 mN, thickness t is 10 μm, and the backside pressure is 30 kPa. This simulation corresponds to the evaluation of two-point discrimination ability of the tactile imager. A parameter of mechanical crosstalk between the two input points is introduced as 'crosstalk ratio' for quantitative evaluation of the spatial resolution. It is determined as a ratio of generated stresses between the input point and the center of the input points when the amplitudes of two input forces are equal. Here, the 'crosstalk length' is determined as the distance at which the crosstalk ratio becomes 0.5. As seen in Fig. 5 (b), the crosstalk ratio becomes approximately 0.5 at 360 μm distance for the boundary condition. If the length d is shorter than 360 μm, crosstalk ratio becomes higher than 0.5. Each peak value at force input point is significantly enhanced by the signal crosstalk, and it is difficult to distinguish the two points of force input. 360 μm is considered as the 'crosstalk length' in this simulation condition. The crosstalk ratio was almost independent of the input force in the simulated range from 0.5 to 15 mN, since it is determined as the ratio of generated stress. On the other hand, the crosstalk ratio has dependence on the backside pressure and diaphragm thickness. If the backside pressure is increased from 30 kPa to 60 kPa, crosstalk ratio is improved by 18.6 % since the deformation around the contact point becomes more local. In this case, the crosstalk length is shortened to below 300 μm. If the thickness of diaphragm is reduced from 10 μm to 5 μm, the crosstalk length of approximately 250 μm can be obtained at 30 kPa backside pressure.

The crosstalk length is a function of both the diaphragm dimensions and the backside pressure. Spatial resolution of the tactile imager is determined either from the crosstalk length or the pixel layout pitch of piezoresistor array.

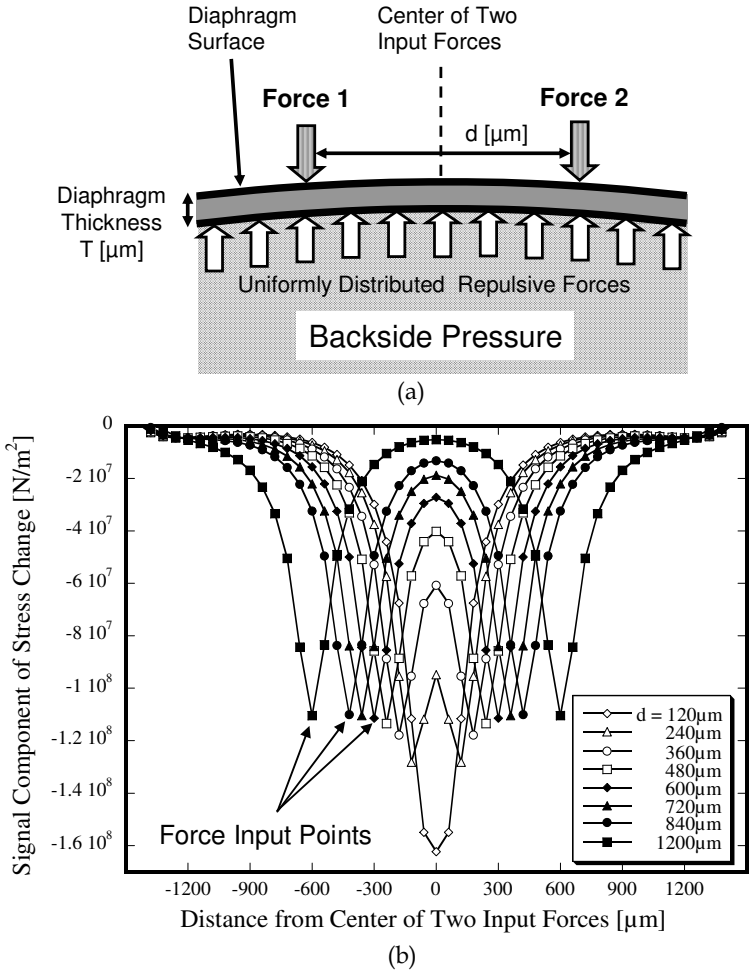

Fig. 5. FEM simulation for spatial resolution analysis; (a) Model parameters in the FEM analysis for the estimation of mechanical crosstalk between two input forces, (b) Distribution of stress signal component generated by the two input forces for various distances of d. The backside pressure is 30 kPa.

As discussed in this section, the backside pressure of the diaphragm influences both the spatial resolution and the sensitivity for contact input forces. A comparison of FEM results simulated at different pressures is helpful to understand this relationship. Figure 6 (a) and (b) show the simulated stress change (signal component) distributions on a sensing diaphragm of this tactile imager at 23.0kPa and 5.0kPa, respectively. A half model of the sensor structure is used. A load of 8.5mN is applied at the contact point in the figure. In the case of 23.0kPa (Fig. 6 (a)), stress change is distributed locally around the contact point. On the other hand, both the stress level and strained area are increased in the 5.0kPa case as shown in Fig. 6 (b). This means that reduction of the backside pressure results in both

improvement of sensitivity (i.e. SNR) and degradation of spatial resolution for an input force applied. Selecting a proper backside pressure adaptively for the device dimensions and expected input force range, the maximum SNR of the tactile imager can be obtained for a required spatial resolution (crosstalk length).

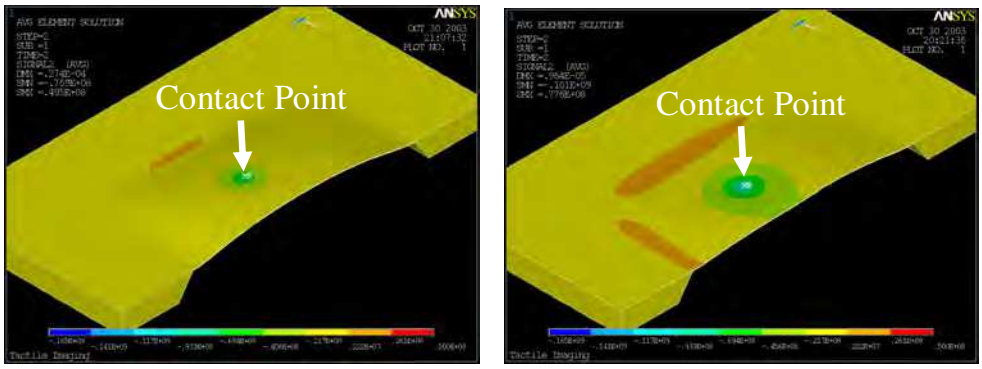

(a) (b)

Fig. 6. Simulated stress change (signal component) distributions on a sensing diaphragm of this tactile imager; (a) Backside pressure is 23.0kPa; (b) Backside pressure is 5.0kPa.

3. Device design and fabrication

3.1 Design of piezoresistor pixel circuit on diaphragm

Signal component of the stress, generated by the object contact, is translated into voltage signal in each pixel circuit with piezoresistor. Figure 7 (a) shows the circuit configuration of each pixel on the diaphragm. A pixel includes n-type diffused piezoresistor for the detection of surface stress (R_{PR}), n^+-poly Si reference resistor with very small stress sensitivity (R_{poly}), logic gates for pixel select operation (NAND and NOT), and switch MOSFETs for resistor drive current (M1) and pixel output (M2). Tensile membrane stress generated strongly on the swollen diaphragm is almost isotropic, and the shear component of stress on each pixel is almost zero. Select terminals of line (*X_Sel*) and column (*Y_Sel*) of pixel circuits in the array is driven sequentially in order to read out the distribution of output voltage. If both *X_Sel* and *Y_Sel* in the pixel are pulled up to V_{dd}, switches M1 and M2 are turned on, and drive current for R_{PR} and R_{poly} is provided from the power source through M1. The piezoresistor R_{PR} translates the surface stress level on each pixel into a corresponding resistance value. Voltage of the output line is determined as a partial voltage of R_{PR} and R_{poly} since M2 is turned on in this case. The output voltage of pixel (V_{Pix_Out}) fed to the common amplifier in the following stage is expressed by the next equation (Takao et al, 2006);

$$V_{Pix\_Out} \approx \frac{R_{Poly} \cdot (V_{DD} - V_{SS})}{R_{PR} + R_{Poly}} \cdot \frac{R_{Amp}}{R_{M2} + R_{Amp}} = \frac{R_{Poly}}{R_{PR} + R_{Poly}} \cdot (V_{DD} - V_{SS}) \quad [\mathrm{V}] \quad (1)$$

where R_{Amp} is equivalent input impedance of the common amplifier (dashed line in the figure), and R_{M1} and R_{M2} are on-channel resistances of M1 and M2, respectively (Takao et al., 2006). In this situation, M1 and M2 are operating in non-saturation region at gate voltage of V_{dd}, and its channel resistance is much lower than the other resistances (i.e. $R_{M1} << R_{PR}$, R_{poly}

and R_{M2}<< R_{Amp}). Assuming that only the planar components of surface stress in parallel to the diaphragm surface is dominant, resistance of a piezoresistor can be expressed with a simplified linear expression with the products of piezoresistive coefficient and applied stress. If n-type piezoresistor in the pixel is integrated on Si(100) and oriented to a direction equivalent to <110>, longitudinal and transversal components of piezoresistive coefficient become equal (i.e. $\pi_{long} = \pi_{trans} = \pi_{n<110>}$) (Kanda, 1982). Resistance value of R_{PR} under tensile membrane stress can be expressed as the following expression considering the isotropic distribution of stress on the swollen diaphragm;

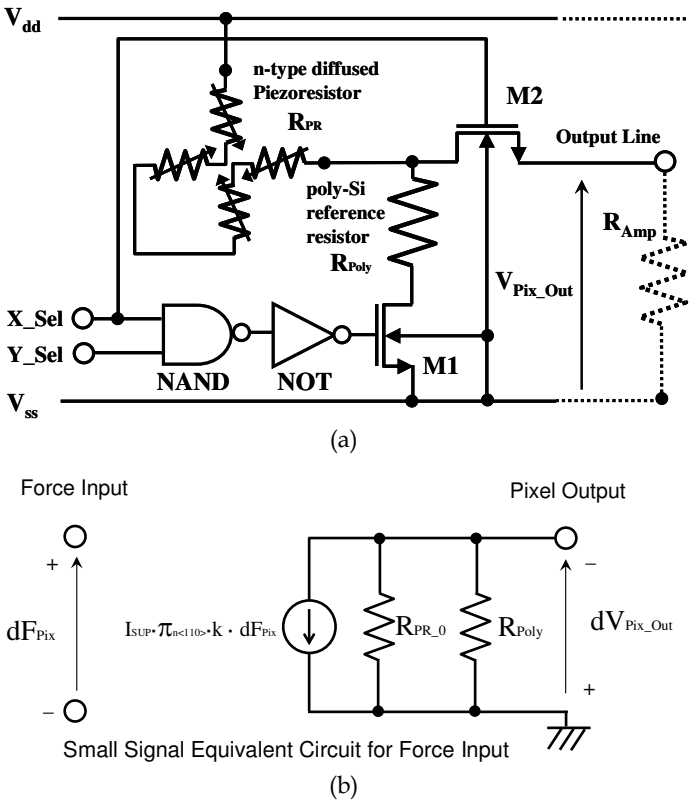

Fig. 7. An example of pixel circuit design including a piezoresistor; (a) Circuit configuration of a unit pixel, (b) Small signal equivalent circuit of the pixel for a force input signal.

$$R_{PR}(\sigma) \approx R_{PR\_0} \cdot (1 + \pi_{long}\sigma_{long} + \pi_{trans}\sigma_{trans}) = R_{PR\_0} \cdot (1 + \pi_{n<110>}\sigma_{EQ}) \quad [\Omega] \quad (2)$$

where R_{PR_0} is the resistance of R_{PR} under zero-stress condition, and σ_{EQ} is an equivalent value of stress corresponding to the sum of the two-axis components of average stress distributed on piezoresistor in a pixel. Typical values for $\pi_{n<110>}$ are around 10^{-10} m^2/N and its polarity is negative. Stress sensitivity of the output voltage in the pixel can be derived by partial differential on σ_{EQ};

$$S_{Pix\_\sigma} = \frac{\partial V_{Pix\_Out}}{\partial \sigma_{EQ}} \approx -\pi_{n<110>} \cdot (V_{DD} - V_{SS}) \cdot \frac{R_{PR\_0} \cdot R_{Poly}}{(R_{PR\_0} + R_{Poly})^2} = -\pi_{n<110>} \cdot I_{SUP} \cdot R_{R_{PR\_0} // R_{Poly}} \quad [\mathrm{V/(N/m^2)}] \ (3)$$

where $R_{RPR\_0//RPoly}$ is the combined resistance of parallel connection of R_{PR_0} and R_{Poly}, and I_{SUP} is the initial supply current to R_{PR} and R_{Poly}. Assuming a linear relationship between average stress change on a pixel and average contact force applied on the pixel area, force sensitivity of the pixel can be expressed as small signal sensitivity in the following expression;

$$S_{Pix\_F} = \frac{dV_{Pix\_Out}}{dF_{Pix}} = \frac{S_{Pix\_\sigma} \cdot d\sigma_{EQ}}{dF_{Pix}} = \frac{S_{Pix\_\sigma} \cdot k \cdot dF_{Pix}}{dF_{Pix}} = -R_{R_{PR\_0} // R_{Poly}} \cdot I_{SUP} \cdot \pi_{n<110>} \cdot k \quad [\mathrm{V/N}] \ (4)$$

where $d\sigma_{EQ} = k \cdot dF_{Pix}$, and k is the conversion factor from the input force (dF_{Pix}) into signal component of stress change on the pixel ($d\sigma_{EQ}$) discussed in the section 2.2. The conversion factor strongly depends on the stiffness of diaphragm surface (i.e. backside pressure). Output signal of a pixel is expressed as a product of S_{Pix_F} and input force.

Figure 7 (b) shows the small signal equivalent circuit of a piezoresistor pixel corresponding to the above relationship between the input force and pixel output. Reading the output signal obtained from sensing pixels in the array, contact force image on the diaphragm can be obtained as two-dimensional distribution. It is easily derived from the simple analysis of the partial differential of pixel sensitivity on R_{PR} that the maximum sensitivity is obtained if the condition $R_{PR} = R_{Poly}$ is satisfied in the real device. Resistance values of R_{PR_0} and R_{Poly} are decided from the power consumption point of view for a fixed power supply voltage and pixel area, while the ratio of resistances should be controlled to bring it close to 1.0 for high sensitivity.

3.2 Layout design of the overall sensor chip

A prototype device with a small scale integrated sensor array was designed and fabricated. The die size of the designed sensor is 5200 × 5200 μm², and the sensing diaphragm region with integrated pixel array is 3040×3040 μm². 5.0μm technology design rule was used in the pixel circuit design, and the size of pixel layout equivalent to Fig. 7 (a) became 420 × 420 μm². R_{PR} and R_{Poly} were designed to be 3 kΩ in the pixel layout. In the prototype device, 6 × 6 sensing pixel array was designed on the sensing diaphragm considering the pixel size (pitch) and the diaphragm size. The sensor array occupies an area of 2520 × 2520 μm² on the diaphragm. Tensile membrane stress becomes quite uniform over the array area, and the effect of fixed diaphragm edge, estimated by FEM simulation, is below 10 % in the area. On the peripheral of the diaphragm region, signal conditioning circuits for sensing operation were designed. It includes array scanning logic circuits for sequential readout of pixel array outputs, a reference signal generator for differential readout of each pixel output.

Diaphragm area in the device is same as in the simulated model discussed in section 2.2. Thickness of the sensing diaphragm of the device was decided considering some parameters. A thinner diaphragm is advantageous to a thicker one for controllability of the mechanical property with air pressure as shown in Fig. 4. Also, the thinner the diaphragm, the higher the spatial resolution as discussed in section 2.2. Considering the advantages, designed pixel size of 420 μm, and some difficulties in fabrication process, the thickness was decided to 10 μm. The spatial resolution of the designed device is considered to be

approximately equal to the pixel size in this design, since the crosstalk length becomes 360 μm at 30 kPa for 10 μm-thick diaphragm, which is shorter than the pixel pitch, 420 μm. If the backside pressure is reduced to below 18 kPa, spatial resolution will be limited by the increased crosstalk length instead of the pixel pitch.
Calculated displacement of the diaphragm at the center is 31.8μm for 30 kPa, and 48.6 μm for 100 kPa backside pressure. Although, the mechanical stroke is too short to apply it to fingertip tactile sensor application, flexibility of the sensor surface is much higher than the conventional silicon-MEMS tactile imagers. The movable distance can be increased using larger and thinner diaphragm structure.

3.3 Device fabrication from standard LSI wafers

The designed device was fabricated with our silicon IC/MEMS fabrication technology (Takao et al., 1997; 1999; 2001). Figure 8 shows outline of the fabrication process. 1) Starting material of the tactile imager was 2-inch and 300 μm-thick p-type Si (100) wafer with resistivity of 1~3 Ω. 2) 6 × 6 Sensing pixel array including piezoresistors and signal processing circuits were fabricated. 3) After the electrical check of the circuits, surface of the integrated circuit was protected by 6 μm-thick polymer layer (CYTOP®) to prevent physical damage in the following bulk-etching process (Takao et al., 1997). The diaphragm etching pattern was defined by SiO_2 layer using wafer backside aligner. 4) Silicon substrate was etched by 25-wt% TMAH solution at 90 °C for 6.5 hours using the SiO_2 masking layer. In this step, silicon thickness of the sensing diaphragm region was controlled to 10 μm ± 1 μm by etching time control. Variation of thickness in a diaphragm was within 0.5 μm. 5) The protective layer on the surface was removed, and a glass substrate with through holes was bonded to the backside of silicon wafer by adhesive bonding with epoxy glue.

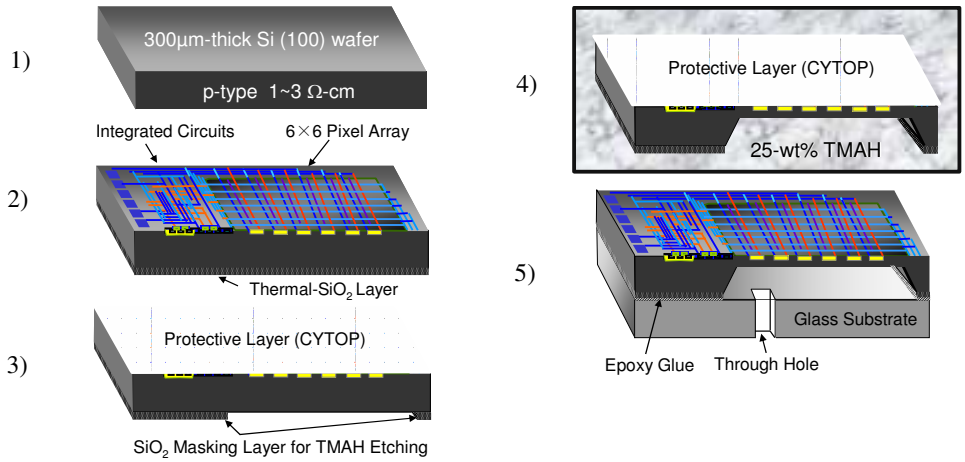

Fig. 8. Fabrication process; 1) Starting material of the tactile imager, 2) Fabrication of 6 × 6 Sensing pixel array including piezoresistors and signal processing circuits, 3) Protection of the circuit surface by a polymer layer (CYTOP®) and definition of the diaphragm etching pattern, 4) Backside-wafer etching with 25-wt% TMAH solution at 90 °C, 5) Removal of the protective layer on the surface and bonding to the glass substrate with epoxy glue layer.

Figure 9 (a) shows a photograph of the fabricated tactile imager with 6 × 6 pixel array integrated on a diaphragm structure. Close-up photograph of a pixel circuit corresponding to Fig. 7 (a) is shown in Fig. 9 (b). In the pixel, n-type piezoresistor device has a box-like shape to detect isotropic stress on the swollen diaphragm effectively, since n-type piezoresistor on Si(100) has bi-axial sensitivity. The areas of the piezoresistor and n^+-poly Si reference resistor are indicated in the figure.

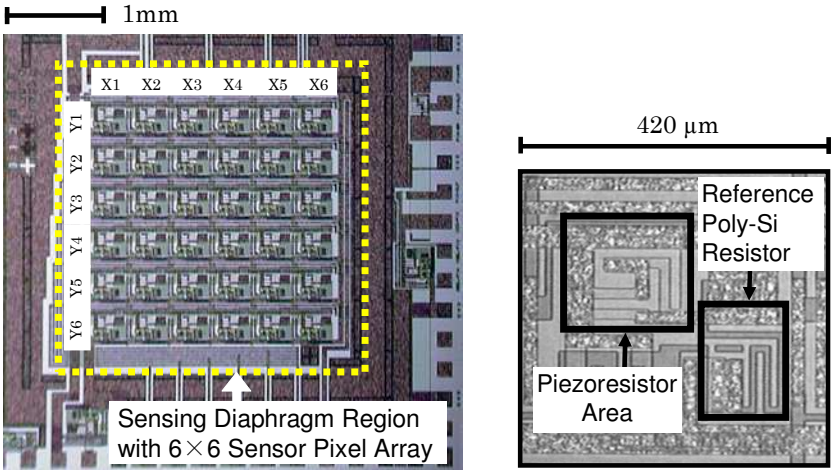

(a) (b)

Fig. 9. Photograph of a fabricated tactile imager with 6 × 6 pixel array integrated on the diaphragm; (a) Overall Chip, (b) Close-up of a pixel circuit in the 6 × 6 pixel array.

4. Characteristics evaluation

4.1 Single point contact force detection

Device characterization was performed with the experimental setup shown in Fig. 10 (a). The fabricated sensor was fixed on a three-axis (X-Y-Z) stage with position resolution of 1 μm in order to control the contact position and input force of measured object on the sensing

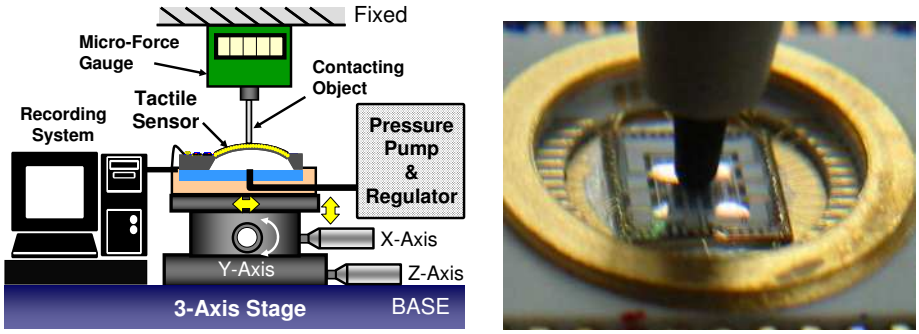

(a) (b)

Fig. 10. Experimental setup; (a) Total system for device characterization; (b) Photograph of a sensing diaphragm deformed by a touching object.

diaphragm. A micro-force gauge with 0.5 mN resolution was used to measure the total contact force of measured object on the sensor surface. Controlled air pressure was applied to the diaphragm backside using a pumping system and a pressure regulator. Signal obtained from the sensor chip was recorded with external measurement equipment and PC. Fig. 10 (b) shows a photograph of the sensing diaphragm deformed by a touching object. Deformation of the diaphragm surface and the indentation can be easily recognized by the reflection of light on the sensing area.

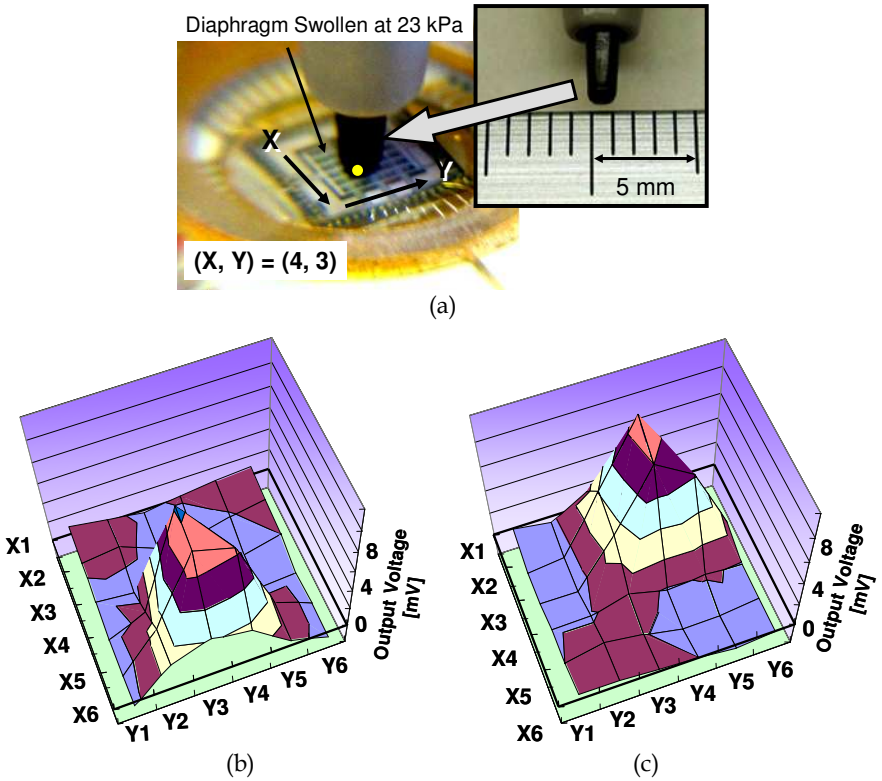

Fig. 11. (a) Photograph of evaluation experiment using a plastic tip with a width of approximately 1mm. The plastic tip is contacting at around (X4, Y3) address in 6×6 array at 29 mN, (b) Measured output voltage mapping of the fabricated prototype device in the case the plastic tip is contacting at around (X4, Y3), (c) Measured output voltage mapping in the case the plastic tip is contacting at around (X2, Y4).

First, the detection ability of single point contact was evaluated. Figure 11 (a) shows the photograph of evaluation experiment using a plastic tip with gentle point as the contacting object. In the photograph, the tip is contacting on a pixel around (X4, Y3) address in 6 × 6 sensor array. A 23.0kPa pressure was applied to the diaphragm backside, and the plastic tip was put on a pixel on the sensing diaphragm with 29mN-force. Movable stroke of the swollen diaphragm from the original surface was approximately 30 μm at the center of the diaphragm. Spatial resolution of the tactile imager is the pixel pitch of 420 μm for 23.0 kPa backside pressure as discussed in the previous section. Considering the movable stroke of

the sensor surface, only a small tip area of the plastic tip is contacting on the diaphragm surface. The width of the tip is approximately 1 mm.
Figures 11 (b) and (c) show measured output voltage mapping obtained from the tactile imager in this experiment. In Fig. 11 (b), since the plastic tip is contacting around (X4, Y3), the peak of the pixel output signal appears on the same address in the 3-D plot. In addition, since the spatial resolution of the tactile imager is 420 μm, contact force applied by the gentle point with 1 mm width is detected by the pixels around (X4, Y3). In other words, the gentle shape wider than the spatial resolution is detected by the plural pixels in the sensor array. After the measurement, the plastic tip was moved to another position (X2, Y4), and the output signal obtained from the sensor is as shown in Fig. 11 (c). The peak position of output signal appears at (X2, Y4), and the shape of peak in the output around the contacting point is similar as in the case of (X4, Y3). Amplitude of the output peak is almost same in these two cases.

4.2 Multi-point contact and 3-D surface shape detection

Multi-point detection ability of this tactile imager was also evaluated. Figure 12 (a) shows a photograph of the multi-point contact test arrangement using two sharp fingers of a rubber toy. The fingers are contacting at the points of (X3, Y2) and (X4, Y5) with total load of 29 mN. The right finger contacting at (X4, Y5) is slightly longer than the left finger contacting at

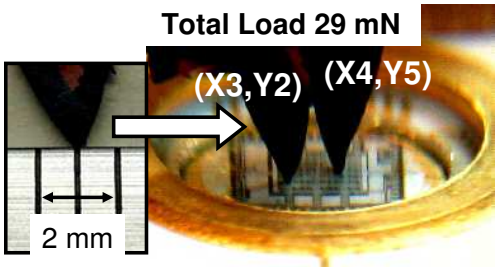

(a)

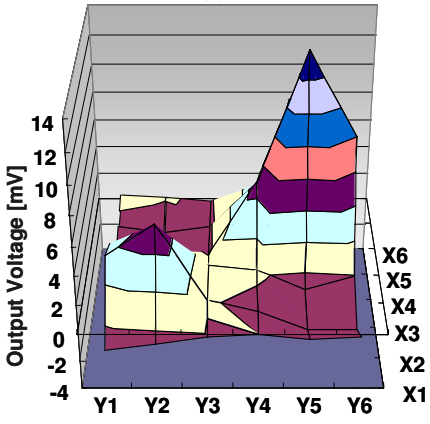

(b)

Fig. 12. Multi-point detection using this tactile image sensor; (a) Photograph of multi-point contact test and the sharp point of the rubber finger. Two fingers of rubber toy are contacting at (X3, Y2) and (X4, Y5), respectively, (b) Obtained output distribution with two signal peaks at (X3, Y2) and (X4, Y5), that correspond to the two positions of touch of the two rubber fingers.

(X3, Y2). As seen in the photograph, the shape of the points of the rubber fingers is much sharper than the point of the plastic-tip shown in Fig. 11 (a). The width of the points is approximately below 300 μm under the contacting situation, and it is smaller than the spatial resolution of the tactile imager (i.e. 420 μm in this experiment). Distribution of the output signal obtained from the experiment is shown in Fig. 12 (b). There are two signal peaks at (X3, Y2) and (X4, Y5), and their positions correspond to the two contact points of the two rubber fingers. Signal level of the peak at (X4, Y5) is larger than the peak at (X3, Y2). This corresponds to the fact that the partial contact force of the rubber finger at (X4, Y5) is larger than that of at (X3, Y2). In addition, the shapes of the output peaks around the contacting positions are much sharper than the shapes obtained in Fig. 11 (b) and (c). This fact implies that the shape of peak point in the output distribution correctly reflects the shape of the contacting point within the limit of the spatial resolution, even though some effect of mechanical crosstalk is seen among the pixels. Through the experiments, basic detection ability of multiple contact forces and the spatial resolution of the tactile imager have been demonstrated successfully.

4.3 Ability of characteristic control

Dependence of the contact force sensitivity of each pixel on the backside pressure was evaluated using a sharp tip of rubber finger shown in Fig. 12 (a), since contacting point smaller than the pixel size is necessary to evaluate the pixel sensitivity. Figure 13 (a) shows a measured relationship between pixel force sensitivity of the fabricated sensor and the diaphragm backside pressure. Supply voltage was 5 V, and piezoresistor pixel at (X3, Y4) was used in the measurement. In the figure, sensitivity dependence on the backside pressure, calculated using FEM, is also plotted. Since the FEM results are additionally plotted to have agreement with the measured sensitivity at 20 kPa, only the shape of pressure dependence can be compared in this figure. Dependence of FEM simulation results on the backside pressure are in good agreement with the measured characteristics. Increasing the pressure, force sensitivity decreased due to increase of repulsive force of the swollen diaphragm. The higher the pressure, the lower the pixel force sensitivity. The force sensitivity is backside pressure dependent, whereas measured noise floor of the pixel output is a constant value (approximately 10 $\mu V/Hz^{0.5}$) and independent of the pressure. Hence, a lower backside pressure results in a higher signal to noise ratio (SNR), and is suitable for the detection of small amplitude of the contact force. For example, the minimum detectable input force becomes approximately 1 mN at 2 kHz bandwidth in the case of 60 kPa backside pressure. This result indicates that if the diaphragm backside pressure is reduced to 5 kPa, the minimum detectable input force will be improved to about 400μN with the same signal bandwidth.

Not only the sensitivity but also the maximum input force is dependent on the backside pressure. If the backside pressure is too low for an input force applied to the sensor surface, the diaphragm yields to the over load. Diaphragm surface is swollen to opposite side by a large input force, and pixel output is finally saturated due to the bottoming of the diaphragm deflection. A higher backside pressure is required to detect and support a larger input force on the diaphragm even if the force sensitivity of pixel (i.e. SNR) is degraded. Figure 13 (b) shows the measured relationships between the forced displacement of diaphragm and pixel input force for various backside pressures. Forced displacement calculated with FEM is also plotted in the figure. Even though there are some differences, the results of FEM show a good agreement with the measurement results. Stiffness of the

diaphragm surface increases as the backside pressure increases. It is clearly expected from the results that the maximum input force of the tactile imager can be increased by increasing the backside pressure. There is a tradeoff relationship between SNR and the input force range in the tactile imager as seen in the experimental results. The lower the backside pressure, the higher the force resolution and the lower the maximum input force. In

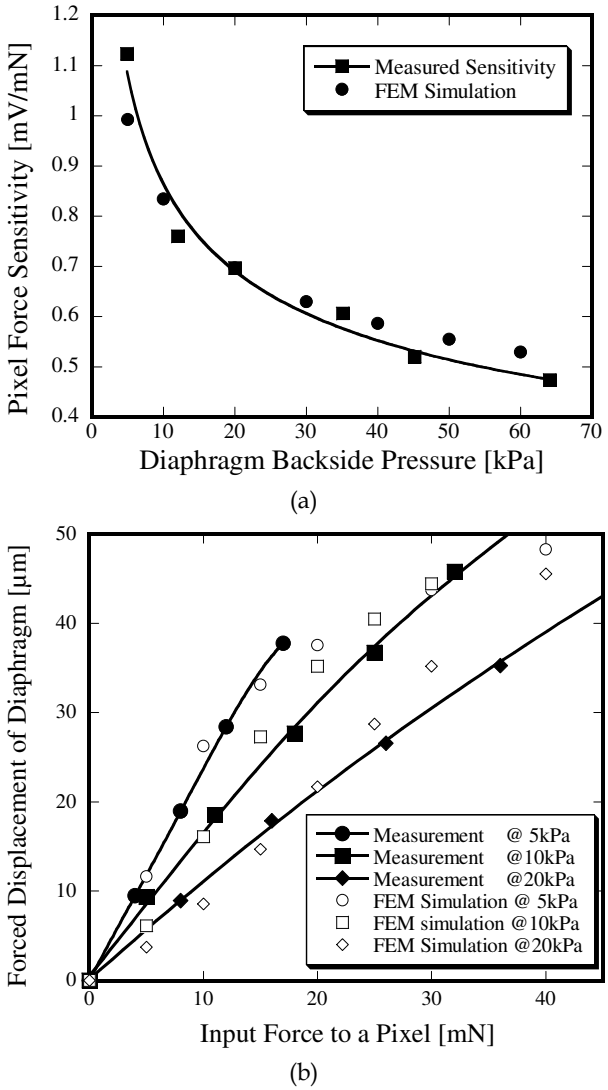

Fig. 13. (a) Measured force sensitivity of a pixel for various diaphragm backside pressures. Simulated sensitivities with FEM non-linear analysis are also plotted, (b) Measured relationship between forced displacement of the diaphragm surface and input force for various backside pressures.

contrast, the higher the backside pressure, the lower the force resolution and the higher the maximum input force. Figure 14 shows an example of over-range input measured with the plastic tip used in Fig. 11. The plastic tip is contacted on (X4,Y5) pixel in the swollen diaphragm at a force of 33mN. The backside pressure is only 4.8kPa which is insufficient for the input. In this case, large area of the diaphragm is largely deformed downward, and precise shape of the tip is not obtained. Once the backside pressure is increased to 23kPa, sharp shape image of the tip is obtained, and contacting position is well recognized similarly with Fig. 11 (b) and (c).

In conclusion, if the backside pressure is adaptively controlled for amplitudes of the input forces, apparent dynamic range of the tactile sensor will be improved. It has been confirmed that the maximum input force range can be controlled from 21 mN to 176 mN by changing the backside pressure from 5 to 64 kPa using the same device (Takao et al., 2006). Even if adaptive control of the pressure is not necessary, sensing characteristics can be chosen or optimized by selecting the sealing pressure suitably for the estimated range of input force in the application.

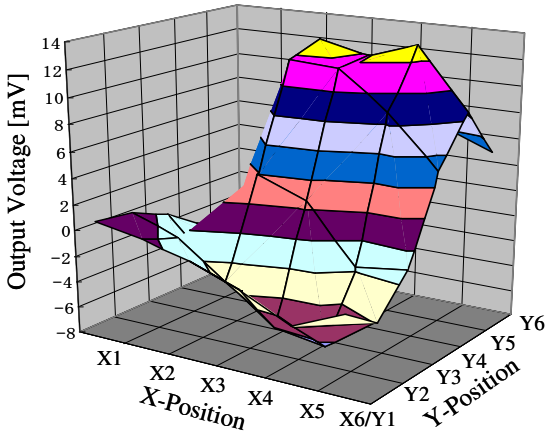

Fig. 14. An example result of over-range input measurement.

5. Conclusions and outlook

In this chapter, a novel concept of silicon-MEMS tactile imager aimed at fingertip tactile applications and evaluation results of a fabricated device have been presented. Array of strain-sensitive sensor pixels was integrated on a pneumatically swollen silicon diaphragm with signal processing circuits in monolithic configuration. Elastic surface of the tactile imager is realized using repulsive force of air pressure applied to the diaphragm backside. Contact force distribution of an object was detected from stress distribution change on the diaphragm. Force range and force sensitivity can be controlled by the pressure even after device packaging step. In this principle, fine pitch of pixels and a large scale sensing array can easily be realized using abilities of silicon CMOS technology. In addition, movable stroke of the sensor surface can be made much longer than individually formed micro mechanical pixels. A designed and fabricated sensor with 3040×3040 μm² sensing diaphragm was fabricated integrating with a 6 × 6 array, 420μm-pitch, piezoresistor pixels.

Movable stroke of the swollen diaphragm from the original surface is around 30 μm at 23 kPa pressure at the center. Realized spatial resolution of the fabricated device is approximately 400 μm, which is determined by the relationship between the pixel pitch and mechanical crosstalk among the pixels. The crosstalk depends on both the diaphragm thickness and backside air pressure. Positions of touch and their contact force amplitudes were detected as 2-D distribution of output voltage form the pixel array in multi-point contact test. The maximum input force range can be controlled from 21 mN to 176 mN by changing the backside pressure from 5 to 64 kPa. Through the evaluation of the fabricated device, advantages of the new configuration of tactile imager have been demonstrated successfully.

As introduced in Section 1, multi-functional sensing is one of future directions for tactile imager devices. Recently, our group has presented multi-functional tactile imager with integrated arrays of piezoresistors and temperature sensors for simultaneous detection of force and temperature distribution images (Takao et al., 2005). Also, another group has succeeded to realize simultaneous measurement of stress and temperature using single field-effect transistor structure (Doelle et al., 2006). Realization of multi-functional detection ability is a firm direction of future technology in integrated silicon smart sensor field. The advantage of silicon technology for integration is very promising feature for highly functional tactile imager for advanced tactile sensing applications. On the other hand, once over-ranged strain is applied, silicon is well known as a fragile material even though it has very good mechanical properties and large breaking stress in room temperature. Research to realize robustness of the silicon tactile imager has just started (Takao et al., 2007), and it will be a challenge to change silicon tactile imagers from a research target to practical sensing devices used widely in many fields.

6. References

Brussel, H. V. &Belien, H. (1986). A High Resolution Tactile Sensor for Part Recognition, *Proc. 6th Int. Conf. Robot Vis. Sens. Control*, pp. 49-59.

Engel, J.; Chen, J. & Liu, C. (2003). Development of polyimide flexible tactile sensor skin, *Journal of Micromechanics and Microengineering*, Vol. 13, No. 9, pp. 359-366.

Engel, J.; Chen, J.; Fan, Z. & Liu, C. (2005). Polymer micromachined multimodal tactile sensors, *Sensors and Actuators A*, Vol. A117, No. 1, pp. 50-61.

Shimojo, M.; Makino, R.; Namiki, A.; Ishikawa, M. & Mabuchi, K. (2004). A Tactile Sensor Sheet Using Pressure Conductive Rubber with Electrical Wires Stitched method, *IEEE Sensors journal*, Vol. 4, No. 5, pp. 589-596.

Someya, T.; Sekitani, T.; Iba, S.; Kato, Y.; Kawaguchi, H. & Sakurai, T. (2004). A large-area, flexible pressure sensor matrix with organic field-effect transistors for artificial skin applications, *Proceedings of the National Academy of Sciences of the United States of America*, Vol. 101, Issue 27, pp. 9966-9970.

Sugiyama, S.; Kawahata, K.; Yoneda, M. & Igarashi, I. (1990). Tactile Image Detection Using a 1k-element Silicon Pressure Sensor Array, *Sensors and Actuators A*, Vol. 22, No. 1/3, pp. 397-400.

Suzuki, K.; Najafi, K. & Wise, K. (1990). A 1024 element high-performance silicon tactile imager, *IEEE Transactions on Electron Devices*, Vol. 37, No. 8, pp. 1852-1860.

Suzuki, K.; Najafi, K & Wise, K. (1990). Process alternatives and scaling limits for high-density silicon tactile imagers, *Sensors and Actuators A*, Vol. 23, No. 1/3, pp. 915-918.

Kobayashi, S.; Mitsui, T.; Shoji, S. & M. Esashi (1990). Two-lead Tactile Sensor Array Using Piezoresistive Effect of MOS Transistor, *Tech. Digest of the 9th Sensor Symposium*, pp. 137-140, Tokyo, Japan, June 1990, IEEJ, Tokyo.

Souza, R. & Wise, K. (1997). A very high density bulk-micromachined capacitive tactile imager, *Digest of Tech. Papers of Transducers'97*, Vol. 2, pp. 1473-1477, Chicago USA, June 16-19, 1997.

Mei, T.; Ge, Y.; Chen, Y.; Ni, L.; Liao, W.; Xu, Y. & Li, W. (1999). Design and Fabrication of an Integrated Three-Dimensional Tactile Sensor for Space Robotic Applications, *Proceedings of IEEE MEMS'99*, pp. 130-134, 1999.

Mei, T.; Ge, Y.; Chen, Y.; Ni, L.; Li, W. J. &Chan, M. H. (2000). An integrated MEMS three-dimensional tactile sensor with large force range, *Sensors and Actuators A*, Vol. A80, No. 2, pp. 155-162.

Sato, N.; Machida, K.; Morimura, H.; Shigematsu, S.; Kudou, K.; Yano, M. & Kyuragi, H. (2003). MEMS fingerprint sensor immune to various finger surface conditions, *IEEE Transactions on Electron Devices*, Vol. 50, No. 4, pp. 1109-1116.

Charlot, B.; Galy, N.; Basrour, S. & Courtois, B. (2004). A Sweeping Mode Integrated Fingerprint Sensor with 256 Tactile Microbeams, *Journal of Microelectromechanical Systems*, Vol. 13, No. 4, pp. 636-644.

Doelle, M.; Peters, C.; Gieschke, P.; Ruther, P. & Paul, O. (2004). Two-Dimensional High Density Piezo-FET Stress Sensor Arrays for In-Situ Monitoring of Wire Bonding Processes, *Proceedings of IEEE MEMS2004*, pp. 829-832, Maastricht The Netherlands, Jan. 25-29, 2004.

Doelle, M.; Held, J.; Ruther, P. & Paul, O. (2006). Simultaneous and Independent Measurement of Stress and Temperature Using a Single Field Effect Transistor Based Sensor, *Proceedings of IEEE MEMS2006*, pp. 150-153, Istanbul Turkey, Jan. 22-26, 2006.

Takao, H.; Matsumoto, Y. & Ishida, M. (1997). A Monolithically Integrated Three Axial Accelerometer Using Stress Sensitive CMOS Differential Amplifiers, *Digest of Technical Papers of Transducers '97*, Vol. 2, pp. 1173-1176, Chicago USA, June 16-19, 1997.

Takao, H.; Matsumoto, Y. & Ishida, M. (1999). An Integrated Three-Axis Accelerometer Using CMOS Compatible Stress Sensitive Differential Amplifiers, *IEEE Transactions on Electron Devices*, Vol. 46, No.1, pp. 109-116.

Takao, H.; Fukumoto, H. & Ishida, M. (2001). A CMOS Integrated Three-Axis Accelerometer Fabricated with Commercial Sub-micron CMOS Technology and Bulk-Micromachining, *IEEE Transactions on Electron Devices*, Vol.48, No.9, pp.1961-1968.

Takao, H.; Sawada, K. & Ishida, M. (2004). Silicon Smart Tactile Image Sensor with Pneumatically Swollen Single Diaphragm Structure, *Proceedings of IEEE MEMS2004*, pp.846-849, Maastricht The Netherlands, Jan. 25-29, 2004.

Takao, H., Sawada, K. & Ishida, M. (2005). Multifunctional Smart Tactile-Image Sensor with Integrated Arrays of Strain and Temperature Sensors on Single Air-Pressurized Silicon Diaphragm, *Dig. Tech. Papers of Transducers'05*, pp. 45-48, Seoul Korea, June 5-9, 2005.

Takao, H.; Sawada, K. & Ishida, M. (2006). Monolithic Silicon Smart Tactile Image Sensor with Integrated Strain Sensor Array on Pneumatically Swollen Single Diaphragm Structure, *IEEE Transactions on Electron Devices*, Vol. 53, No. 5, pp. 1250-1259.

Takao, H.; Yawata, M.; Sawada, K. & Ishida, M. (2007). A Robust and Sensitive Silicon-MEMS Tactile-Imager with Scratch Resistant Surface and Over-Range Protection, *Dig. Tech. Papers of Transducers'07*, pp. 1465-1468, Lyon France, June 10-14, 2007.

Hasegawa, Y.; Shimizu, T.; Miyaji, T.; Shikida, M.; Sasaki, H.; Sato, K. & Itogigawa, K. (2003). Hardness Detection Using A Micromachined Active Tactile Sensor, *Digest of Technical Papers of IEEE Transducers'03*, pp. 927-930, Boston USA, June 2003.

Kanda, Y. (1982). A Graphical Representation of the Piezoresistance Coefficients in Silicon, *IEEE Transactions on Electron Devices*, Vol. ED-29, No. 1, pp. 64-70.

Sensors: Focus on Tactile Force and Stress Sensors

Edited by Jose Gerardo Rocha and Senentxu Lanceros-Mendez

ISBN 978-953-7619-31-2
Hard cover, 444 pages
Publisher InTech
Published online 01, December, 2008
Published in print edition December, 2008

This book describes some devices that are commonly identified as tactile or force sensors. This is achieved with different degrees of detail, in a unique and actual resource, through the description of different approaches to this type of sensors. Understanding the design and the working principles of the sensors described here requires a multidisciplinary background of electrical engineering, mechanical engineering, physics, biology, etc. An attempt has been made to place side by side the most pertinent information in order to reach a more productive reading not only for professionals dedicated to the design of tactile sensors, but also for all other sensor users, as for example, in the field of robotics. The latest technologies presented in this book are more focused on information readout and processing: as new materials, micro and sub-micro sensors are available, wireless transmission and processing of the sensorial information, as well as some innovative methodologies for obtaining and interpreting tactile information are also strongly evolving.

How to reference

In order to correctly reference this scholarly work, feel free to copy and paste the following:

Hidekuni Takao and Makoto Ishida (2008). Three-Dimensional Silicon Smart Tactile Imager Using Large Deformation of Swollen Diaphragm with Integrated Piezoresistor Pixel Circuits, Sensors: Focus on Tactile Force and Stress Sensors, Jose Gerardo Rocha and Senentxu Lanceros-Mendez (Ed.), ISBN: 978-953-7619-31-2, InTech, Available from: http://www.intechopen.com/books/sensors-focus-on-tactile-force-and-stress-sensors/three-dimensional_silicon_smart_tactile_imager_using_large_deformation_of_swollen_diaphragm_with_int

INTECH
open science | open minds

InTech Europe
University Campus STeP Ri
Slavka Krautzeka 83/A
51000 Rijeka, Croatia
Phone: +385 (51) 770 447
Fax: +385 (51) 686 166
www.intechopen.com

InTech China
Unit 405, Office Block, Hotel Equatorial Shanghai
No.65, Yan An Road (West), Shanghai, 200040, China
中国上海市延安西路65号上海国际贵都大饭店办公楼405单元
Phone: +86-21-62489820
Fax: +86-21-62489821